Biochimica et Biophysica Acta 1788 (2009) 936–944

Contents lists available at ScienceDirect

Biochimica et Biophysica Acta

journal homepage: www.elsevier.com/locate/bbamem

Functional equivalence of the nicotinic acetylcholine receptor transmitter binding sites in the open state

Mathew Tantama, Stuart Licht *

Department of Chemistry, Massachusetts Institute of Technology, 77 Massachusetts Avenue, Building 16, Room 573B, Cambridge, Massachusetts 02139, USA

ARTICLE INFO

Article history:
Received 30 July 2008
Received in revised form 14 December 2008
Accepted 21 January 2009
Available online 18 February 2009

Keywords:
Nicotinic receptor
Single-channel
Binding
Conformational change
Open state

ABSTRACT

The subunits of the muscle-type nicotinic acetylcholine receptor (AChR) are not uniformly oriented in the resting closed conformation: the two α subunits are rotated relative to its non-α subunits. In contrast, all the subunits overlay well with one another when agonist is bound to the AChR, suggesting that they are uniformly oriented in the open receptor. This gating-dependent increase in orientational uniformity due to rotation of the α subunits might affect the relative affinities of the two transmitter binding sites, making the two affinities dissimilar (functionally non-equivalent) in the initial ligand-bound closed state but similar (functionally equivalent) in the open state. To test this hypothesis, we measured single-channel activity of the αG153S gain-of-function mutant receptor evoked by choline, and estimated the resting closed-state and open-state affinities of the two transmitter binding sites. Both model-independent analyses and maximum-likelihood estimation of microscopic rate constants indicate that channel opening makes the binding sites' affinities more similar to each other. These results support the hypothesis that open-state affinities to the transmitter binding sites are primarily determined by the α subunits.

1. Introduction

One of the central aims in nicotinic acetylcholine receptor (AChR) physiology and pharmacology is to understand the dynamic interaction between ligands and the transmitter binding sites (TBSs) in the major AChR conformations: the resting closed state (also referred to as the resting state), the open ion-conducting state, and the desensitized closed state (also referred to as the desensitized state) [1]. To develop small-molecule agonists and antagonists with therapeutic potential, it would be useful to understand the state-dependent structural contributions to ligand binding at the TBSs. Biophysical, biochemical, and electrophysiological methods have been used to investigate agonist and antagonist binding to the AChR [1–6], including cryoelectron microscopy of the intact AChR [7], X-ray crystallography of acetylcholine-binding proteins (AChBPs) that are homologous to the intact receptor's TBSs [8–10], X-ray crystallography of the mouse AChR α subunit extracellular domain [11], and X-ray crystallography of a pentameric prokaryotic ligand gated channel structurally similar to AChR models [12]. These structural studies have provided high-resolution models of the agonist-free and agonist-bound receptor; however, there are currently no high-resolution structures of the intact AChR in the functionally relevant agonist-bound resting and agonist-bound open states [2]. The desensitized closed conformations that predominate when agonist is continuously present for long durations (~100 ms or more) are more accessible (and interesting in their own right), but are likely to differ significantly in structure from the resting closed state [13]. Capturing the molecular details of ligand interactions in the transient open state therefore remains a challenging task.

One major conformational change that has been proposed to occur when the AChR opens is the rotation of the α subunits. The muscle-type AChR is a pentameric complex made up of two α subunits, one β subunit, one δ subunit, and either one ε or one γ subunit, arranged in clockwise order αβδαε(γ) when viewed from the synaptic cleft. Cryoelectron microscopy experiments have shown that in the resting closed state, the α subunits overlay well with one another, and the non-α subunits overlay well with one another; however, the α subunits do not overlay well with the non-α subunits [7]. This non-equivalence of subunit orientation in the AChR tertiary structure occurs because the α subunits' interior β-sheets are rotated approximately 10°. In the open state, a 9 Å-resolution model suggests the α subunits rotate such that all subunits overlay well, and the open AChR is highly uniform with respect to subunit orientations (Fig. 1) [14]. Molecular dynamics has also furnished useful insights into mechanisms of channel gating [15]. In the case of the AChR, molecular dynamics studies support the proposal that twisting or tilting reorientations of the M1 and M2 helices occur in the gating conformational change for muscle type [16] and α7 [17] receptors.

If tertiary subunit orientations directly affect the structure of the transmitter binding sites, the state-dependent change in the uniformity of subunit orientations would predict a state-dependent change in the uniformity of binding site affinities, because the α subunits make up part of the TBSs. The adult muscle-type AChR's two

* Corresponding author. Tel.: +1 617 452 3525; fax: +1 617 258 7847.
E-mail address: lichts@mit.edu (S. Licht).

0005-2736/$ – see front matter © 2009 Elsevier B.V. All rights reserved.
doi:10.1016/j.bbamem.2009.01.009

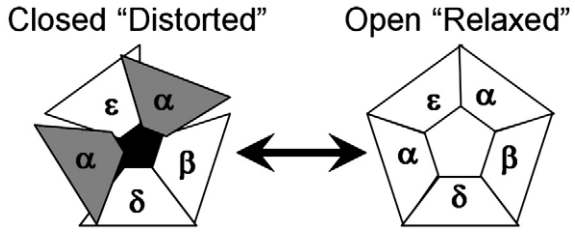

Fig. 1. The relationship between structural and functional equivalence of transmitter binding sites. Rotation of the α subunits causes the orientationally non-uniform closed AChR to become orientationally uniform in the open state.

transmitter binding sites (TBSs) are situated at the α-δ and α-ε subunit interfaces in the ligand-binding domain. Each TBS has a "principal face" made up of Loops A–C and a "complementary face" made up of Loops D–G [1]. The δ and ε subunits contribute the complementary components at their respective TBSs, and the α subunits contribute the principal components at both TBSs. State-dependent conformational changes in the α subunits may therefore affect the TBSs' resting-state and open-state binding affinities.

There are three plausible hypotheses for how the gating conformational change might affect the relative affinities of the two TBSs. First, the difference in the TBSs' open-state affinities (measured as J_d, the dissociation constant for binding to the open conformation) might be larger than the difference in their resting-state affinities (measured as K_d, the more familiar dissociation constant for binding to the resting closed conformation). Because the two TBSs differ structurally in their complementary faces, this observation would suggest that the complementary faces increase their contributions to agonist binding in the open state. Second, the difference in affinities might remain the same in the resting and open states. This observation would suggest that increased open-state affinity is due to improved binding to both faces. Third, the difference in open-state affinities might be smaller than the difference in their resting-state affinities. Because the two TBSs have identical principal faces, this observation would suggest that the principal faces increase their contributions to binding in the open state. We hypothesize that the third possibility is correct: the resting AChR TBSs are structurally and functionally non-equivalent, while the open AChR, in which subunit orientations are more uniform, has TBSs that are equivalent with respect to open-state affinities. Formally, the subunit orientations need not be correlated with the affinities of the TBSs, but the importance of the subunit rotations for gating suggests that a structure–function relationship may exist in which the rotation of the two α subunits affects the two different agonist binding site environments.

Previous work suggests that the difference in resting closed state affinities between the sites can be significant, but that differences in desensitized state affinities tend to be small. Functional studies on intact receptors from a variety of species and subtypes have shown that the resting-state binding sites are functionally non-equivalent with respect to their affinities and association/dissociation kinetics [18–23]. Although the two TBSs of the adult-type AChR have similar resting-state affinities for acetylcholine [19], they have distinctly dissimilar affinities for other agonists such as epibatidine [24]. In the desensitized state, ligand-binding and stopped-flow fluorescence experiments on intact receptors indicate that the differences between the two sites are much smaller [25,26]. However, information about agonist binding in the transient open state has not been easily accessible in functional studies, and it is not clear what differences there may be between the open and desensitized states.

To test the hypothesis that the two TBSs have equivalent binding affinities in the open state, we carried out an analysis of single-channel kinetics for the αG153S gain-of-function mutant and αG153S/wild-type hybrid channels. The αG153S mutant [20,27] permits a larger range of activity to be studied than the wild-type, and it preserves the topography of subunit–subunit interactions in the wild-type receptor by virtue of having the mutated residue in the α subunit. The kinetics of activation of this mutant using acetylcholine [19] and choline have previously been reported [19,20,27], but the thermodynamics of binding to the open state were not investigated. The low-efficacy agonist choline was used in combination with the αG153S mutant because it stimulates gating that is not faster than conventional patch-clamp recording bandwidth [28–30], while retaining the gating mechanism observed for stronger agonists [31]. For choline-evoked αG153S AChR currents, a model-free analysis of open probabilities and dwell times supports the hypothesis that the TBSs are functionally non-equivalent in the resting, diliganded (but non-desensitized) closed state but equivalent in the open state. Maximum-likelihood model fitting of single-channel activity was then used to determine resting-state and open-state affinities. The results of the model fitting support the hypothesis that the thermodynamics of binding reactions differ substantially for the two TBSs in the ligand-bound resting state but become equivalent in the open state. One possible explanation for the functional equivalence of binding sites in the open state is that open-state affinities are primarily determined by the α subunits, a conclusion that is consistent with existing structural data.

2. Materials and methods

2.1. AChR expression

Cell culture reagents were from Invitrogen (Carlsbad, CA). Plasmids for expression of the α, β, δ, and ε subunits were generously provided by Professor Anthony Auerbach (SUNY Buffalo, Buffalo, NY) [19,32]. The αG153S mutation was engineered by site-directed mutagenesis using a Qiagen QuickChange Kit (Valencia, CA) [19,20,27]. Plasmid sequences were confirmed by dideoxy sequencing at the MIT Biopolymers Laboratory (Cambridge, MA).

HEK-293 human embryonic kidney cells (ATCC CRL-1573) were maintained in Dulbecco's Minimum Essential Media (DMEM) supplemented with 10% Fetal Bovine Serum (FBS) at 37 °C in a 5% CO_2 humidified atmosphere. Cells were transfected at 40–60% confluency using the method of calcium phosphate precipitation according to previously published protocols [19]. For one 35 mm dish, a total of 3.5 μg of plasmid DNA was used in a mass ratio of 2:1:1:1 of α:β:δ:ε subunits. Media was changed 8–30 h after addition of DNA, and patch-clamp experiments were conducted 24–72 h after media change.

2.2. Patch-clamp recordings

Choline chloride was obtained from Sigma (St. Louis, MO). Single-channel recording was performed in the cell-attached mode according to previously published protocols [33,34]. The bath solution was Dulbecco's Phosphate Buffered Saline (DPBS) containing (in mM): 137 NaCl, 0.9 $CaCl_2$, 0.5 mM $MgCl_2$, 2.7 KCl, 1.5 KH_2PO_4, 8.1 Na_2PO_4, pH 7.3.

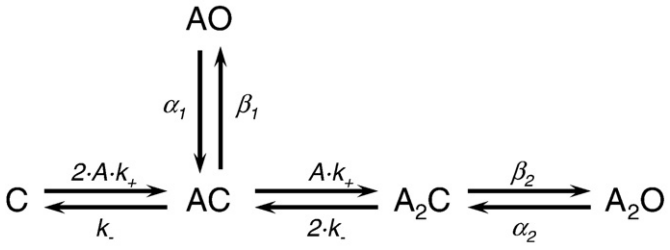

Scheme 1. An AChR kinetic model with binding sites constrained to be functionally equivalent. Conformational states: "C", closed; "O", open; "A" represents bound agonist. Rate constants are in s^{-1} except where noted: β_1, monoliganded opening; β_2, diliganded opening; α_1, monoliganded closing; α_2 diliganded closing; k_+, agonist association ($M^{-1}\cdot s^{-1}$); k_-, agonist dissociation.

Pipette solutions were DPBS supplemented with choline. Membrane potentials were typically −30 to −40 mV, and pipettes were held at a command voltage of −70 mV during recording. Single-channel currents were amplified with an Axopatch 200B (Axon Instruments, Foster City, CA) and recorded through a low-pass Bessel filter at 10 kHz. Data were digitized at a sampling rate of 20–100 kHz using a NI 6040 E Data Acquisition Board (National Instruments, Austin, TX). Data were recorded using QuB software (www.qub.buffalo.edu) [35–39] and re-sampled to 20 kHz during idealization for consistency when necessary. The baselines of single-channel records were adjusted manually using QuB. A 5 kHz Gaussian digital filter was applied, and records were idealized using either the segmental *k*-means or half-amplitude algorithms in QuB [35]. All records were examined visually in their entirety, and misidealizations were corrected manually.

2.3. Kinetic analysis

Analysis of single-channel clusters was performed as previously described [19,34,40]. At high agonist concentrations, single-channel activity occurs as clusters of openings and closings that represent activity from one AChR. Each cluster is a series of openings flanked by long closed durations in which all channels are desensitized. These flanking desensitized durations are longer than a critical time (τ_{crit}). The value of τ_{crit} is assigned between the major closed component (non-desensitized sojourns) and its successor in closed-time distribution. The major closed component scales with agonist concentration and reflects transitions between AChR resting and open conformations, including binding and gating steps. The value of τ_{crit} was chosen to minimize the percentage of misclassified events, and the fraction of misclassified events was typically less than 5%. Performing the kinetic analysis on clusters of events allows transitions between open states and resting (non-desensitized) closed states, rather than desensitized closed states, to be selected for measurement of rate constants. Clusters with multiple-conductance levels (more than one channel) or fewer than five events were excluded. Homogeneous clusters were used if their activity fell within 1–2 standard deviations (SDs) of the mean current amplitude, mean closed time, and mean open time [19]. Single-channel clusters recorded at 0.25, 0.5, 1, 2, and 5 mM choline were globally fitted to AChR gating models (Schemes 1 and 2), using the maximum interval likelihood algorithm with missed event correction. A dead time of 2.5 times the sampling interval was imposed. Fitting was repeated multiple times (10–50 repetitions) for each model with rate constant perturbations to provide higher confidence that the fitted model did not represent erroneous convergence. An additional gap state has been previously described and used in AChR gating models [19]; however, a gap state did not significantly improve fitting here. Other models incorporating choline-dependent block or additional diliganded open states also did not improve fitting.

2.4. Justification for assuming the AChR obeys detailed balance

Detailed balance requires that the AChR operate at thermodynamic equilibrium in the absence of a source of additional free energy. For the AChR, which has no enzymatic component, this free energy can only come from the ion gradient. Binding of a permeant ion to the channel pore might affect gating and cause violations of detailed balance. However, AChR permeant ion block is not detected in single-channel recordings, suggesting the ion gradient is not coupled to AChR gating. Consistent with this hypothesis, previous studies have not detected the temporal asymmetries in bursts of openings that would be expected for violations of detailed balance [41].

3. Results

To determine if the TBSs are functionally non-equivalent in the resting closed state and functionally equivalent in the open state, we performed kinetic analysis on hybrid channels formed from mixing wild-type and G153S mutant α subunits and analyzed open lifetimes of fully mutant channels without assuming a specific kinetic model. Two types of hybrid channel can be functionally expressed, since the mutant α subunit may be adjacent to the δ or the ε subunit. If the binding sites are functionally non-equivalent, these hybrids are expected to exhibit distinct kinetic properties, while if the sites are functionally equivalent, the hybrids are expected to exhibit similar or indistinguishable kinetic properties. As a further test of the functional equivalence between TBSs, we estimated the affinities of the resting closed state and open states using maximum likelihood model fitting and rate estimation.

3.1. Analysis of hybrid channels

To determine the state-dependent changes in functional equivalence with respect to the TBSs, we first analyzed the activity of hybrid channels containing a wild-type and a mutant α subunit. Functional non-equivalence of the TBSs in the resting closed state has been established previously through biochemical and electrophysiological studies [18–24,42], but functional equivalence of the TBSs in the open

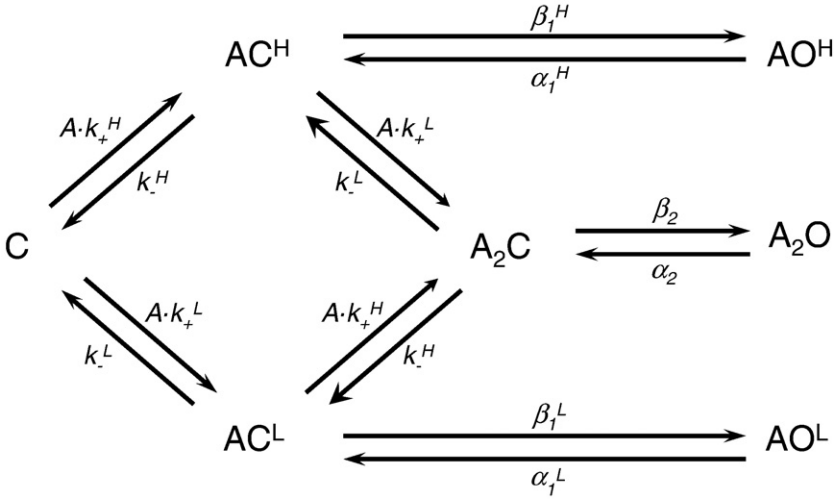

Scheme 2. AChR kinetic model permitting non-equivalence of the binding sites. Low- and high-affinity sites and associated rate constants are denoted by superscript "L" and "H", respectively.

state has not been investigated. One method for examining functional equivalence of the TBSs is the analysis of hybrid channels formed from mixtures of wild-type and mutant α subunits. For example, it has previously been reported that the TBSs are non-equivalent in the resting closed state and contribute unequally to gating [42]. Our results corroborate previous reports indicating the resting TBSs are functionally non-equivalent and provide new evidence that the open-state TBSs are functionally equivalent.

Currents were recorded from cells expressing both the wild-type α and mutant αG153S subunits, along with wild-type β, δ, and ε subunits. Because muscle-type AChRs contain two α subunits, channels can assemble in which both binding sites are wild-type, both sites are mutated, the α-δ site is mutated (hybrid$_\delta$), or the α-ε site is mutated (hybrid$_\varepsilon$) [42]. Currents were recorded at 20 mM choline (4 patches) to saturate the receptors [28]. Four distinct modes of channel activity were observed in the distribution of open probabilities (Fig. 2). For equivalent sites that contribute equally to gating, single-channel activity from the two hybrid populations would be indistinguishable, as has been observed for transmembrane-region mutants [43–45]. In this case, three modes of activity would be observed: wild-type, hybrid, and mutant. In contrast, for non-equivalent sites that contribute unequally to gating, two distinguishable subsets of hybrid channel activity are predicted [42,45], leading to a prediction of four distinct modes of activity. Four modes of activity were observed, and a segmental *k*-means algorithm was used to fit the open probabilities to four Gaussian curves: wild-type, $P_o = 0.12 \pm 0.02$; hybrid, $P_o = 0.33 \pm 0.04$; hybrid, $P_o = 0.54 \pm 0.04$; and mutant, $P_o = 0.80 \pm 0.03$ (mean ± standard error) (Fig. 2). These results show that the TBSs contribute unequally to gating with the αG153S mutant in the presence of choline, consistent with previous results using αD200N and acetylcholine [42].

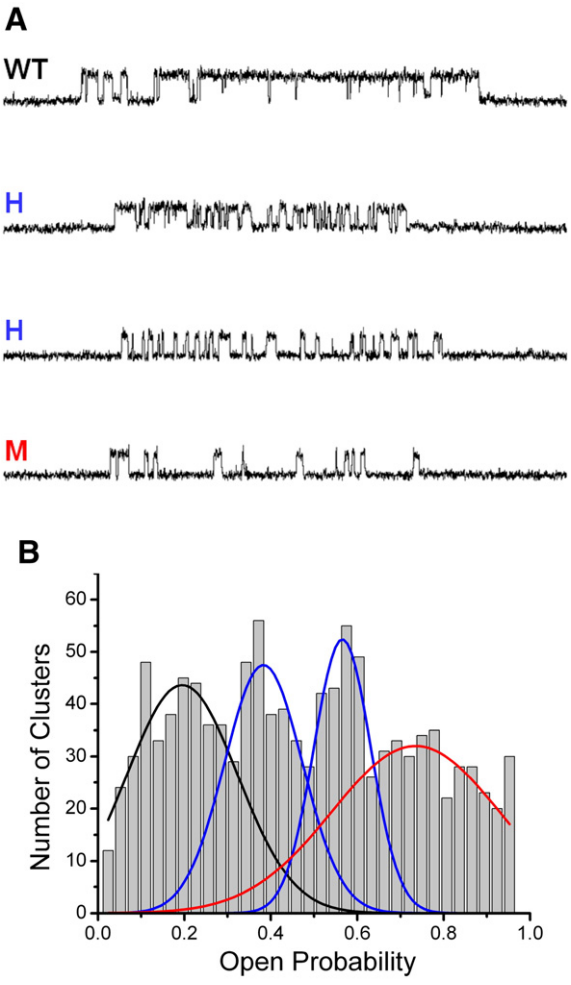

Fig. 2. Hybrid activity from mixtures of wild-type and the G153S mutant α-subunits. (A) Typical clusters of the four modes of activity from wild-type (WT), hybrid (H), and mutant (M) channels elicited at saturating 20 mM choline. (B) A histogram of intracluster open probabilities showing four modes of activity. Data are from a typical recording. A segmental *k*-means algorithm was used to fit four Gaussian curves to the wild-type (black), hybrid (blue), and mutant (red) open probabilities.

Table 1
Maximum likelihood rate estimation of hybrid activity

	θ_2	β_2 (s^{-1})	α_2 (s^{-1})
Wild-type	0.15 ± 0.01	130 ± 40	900 ± 300
Hybrid	0.46 ± 0.04	250 ± 60	500 ± 100
Hybrid	1.1 ± 0.1	500 ± 100	500 ± 100
Mutant	2.8 ± 0.2	1300 ± 400	500 ± 200

To determine the functional equivalence of the TBSs in the open state, gating rate and equilibrium constants of the four populations were determined (Table 1). Although two hybrid activities were observed, the hybrid closing rate constants are equal, consistent with functionally identical open-state TBSs. Only one open lifetime was necessary to fit the experimental distribution of hybrid openings. However, two distinct open lifetimes might be too similar in magnitude to distinguish. The ratio of the two hybrid lifetimes is 1.1 ± 0.1 (mean ± standard error), indicating that if there are two distinct lifetimes, they are unlikely to differ by more than 20–30%.

Because the currents analyzed above were recorded at 20 mM choline to saturate receptors, unresolved fast blockade prolongs the apparent open events, resulting in underestimation of the diliganded closing rate α_2 by 2-fold [28]. However, this phenomenon occurs for all four receptor populations. It therefore does not affect the number of kinetic components observed.

3.2. Analysis of open lifetimes

To further test the functional equivalence of the open state in a model-independent analysis, we analyzed unliganded, monoliganded, and diliganded open lifetimes of the αG153S mutant receptor. The hypothesis of functional non-equivalence in the open-state binding sites predicts that there are four AChR open states: an unliganded state, two distinct hybrid monoliganded states, and the diliganded state. For functionally equivalent open-state binding sites, only three open states are predicted, since the monoliganded states will be identical.

To determine the number of open states and their associated lifetimes, single-channel activity was measured at low choline concentrations (numbers of patches: 1 at 1 nM, 7 at 10 nM, 7 at 100 nM, 5 at 1 μM, 6 at 10 μM; 26 patches total). At low choline concentrations, single-channel activity is not clustered, and resting closed and desensitized sojourns cannot be distinguished. Thus, only open dwell-time distributions and their exponential open time components were analyzed (Fig. 3).

Open events could be classified into short (0.14 ± 0.02 ms, mean ± SD), intermediate (0.6 ± 0.1 ms), and long (1.2 ± 0.2 ms) lifetimes, consistent with prediction of three distinct states for equivalent open-state binding sites. The relative amplitudes of these open lifetimes were concentration dependent (Fig. 3). The short-lifetime open state steadily decreased in relative amplitude with increasing concentration. For the intermediate-lifetime open state, the relative amplitude exhibited a bell-shaped concentration dependence with a maximum at ~10^{-5} –10^{-4} M. The long-lifetime open state was absent at very low concentrations and steadily increased in relative amplitude with increasing concentration. The magnitude of the three open lifetimes and the concentration dependences of their relative amplitudes indicate that they correspond to openings of the unliganded, monoliganded, and

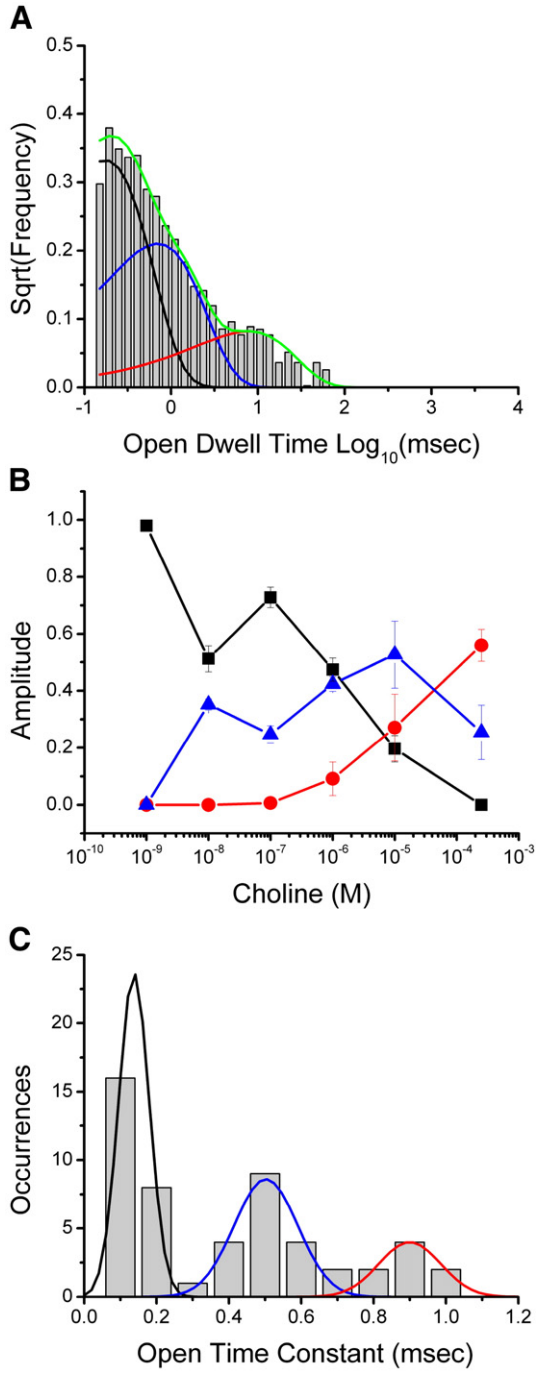

Fig. 3. Estimation of channel closing rate constants at low choline concentrations for the αG153S mutant. (A) A typical open dwell-time distribution obtained at 100 nM choline. The distribution was fitted best by three exponential components, also referred to as time constants. (B) Concentration dependence of the amplitudes for time constants assigned to unliganded (black squares), monoliganded (blue triangles), and diliganded (red circles) openings. (C) A histogram of observed open time constants shows three distinct peaks assigned to unliganded (black), monoliganded (blue), and diliganded (red) openings.

diliganded αG153S AChR. The shortest lifetime is consistent with the reported unliganded lifetime [27] and can be assigned to the unliganded open state, in accord with the observation that increasing choline concentrations decrease the relative amplitude of this kinetic component. The longest lifetime is similar to the lifetime observed at saturating choline concentrations (Table 1) and can be assigned to the diliganded open state, consistent with the observation that increasing choline concentrations favor the longest open lifetime. The monoliganded open state is unlikely to have a lifetime shorter than the unliganded open state or longer than the diliganded open state. The intermediate open lifetime therefore can be assigned to a monoliganded open state, consistent with the observed bell-shaped concentration dependence.

A histogram of the open lifetimes observed in all the low concentration records clearly shows three peaks (Fig. 3). A Gaussian was fitted to each peak, and the channel closing rate constants were determined: the unliganded closing rate constant α_0 (7000 ± 1000 s^{-1}), the monoliganded closing rate constant α_1 ($1900 \pm 400\ s^{-1}$), and the diliganded closing rate constant α_2 ($1100 \pm 200\ s^{-1}$). It is not surprising that the unliganded and monoliganded open states are easily observable, as other gain-of-function mutants have shown a propensity for opening with fewer than two agonist molecules bound [46].

Notably, only one monoliganded open lifetime was observed, consistent with the hypothesis that the open-state TBSs are functionally identical. Additional monoliganded open states were not necessary given the number of events fitted. These data do not rule out the hypothesis that there are two distinct monoliganded open states, but these states would have lifetimes that differ by 10% or less (as judged by least-squares fitting of the histogram in Fig. 3).

3.3. Maximum-likelihood model fitting and rate estimation

To investigate the functional equivalence of the TBSs with respect to resting closed-state and open-state affinities, maximum likelihood model fitting and rate estimation was carried out. We examined two commonly used types of AChR kinetic models: a model which requires functionally equivalent binding sites (Scheme 1) [47] and a model which does not require functionally equivalent binding sites (Scheme 2) [19,20,48,49]. Both models are physically reasonable, and it is important to note that Scheme 2 allows for but does not require the possibility of non-equivalent affinities. Scheme 1 is often a good model for adult muscle-type AChR activity, because the two TBSs have similar resting closed-state agonist affinities for acetylcholine. However, several observations suggest Scheme 2 may be appropriate for analyzing our system. First, the αG153S mutant receptor appears to have distinct resting closed-state affinities for the two TBSs [19]. Second, mutant cycle analysis and the rate-equilibrium free energy relationship suggest that the αG153S mutation does not cause binding site coupling or change the allosteric gating mechanism (Supplementary information). Third, time constant analysis of resting closed times measured from clusters evoked at 0.25 mM choline were fitted best with four closed components, indicating two distinct binding steps may be kinetically distinguishable (Supplementary information). We performed maximum likelihood fitting of both models to establish that Scheme 2 is appropriate for estimating resting closed-state and open-state affinities. While recent results support the hypothesis that a second short-lived closed state (or "flip" state) is an intermediate on the gating pathway [50], the simpler model of Scheme 2 is sufficient to describe the data recorded under our experimental conditions, so we have chosen not to use a more complex model. Since use of the "flip" model yields gating rate constants that are relatively insensitive to structural perturbations in agonists, the open-state affinities we estimate here might be considered apparent affinities for the flip state if interpreted in the context of the "flip" model. Regardless of the model used, however, we have measured affinities in two distinct and pharmacologically important conformations.

To enable the fitting of the multi-state models employed [19,47], model-independent measurements of β_2, α_1, and α_2 were used to constrain the fits. To determine diliganded gating rate constants (β_2 and α_2), clustered single-channel activity was recorded at high concentrations of choline (numbers of patches: 4 at 0.25 mM, 4 at 0.5 mM, 4 at 1 mM, 5 at 2 mM, 4 at 5 mM; 21 total) and the dose–response curves were analyzed (Fig. 4A). The apparent opening rate,

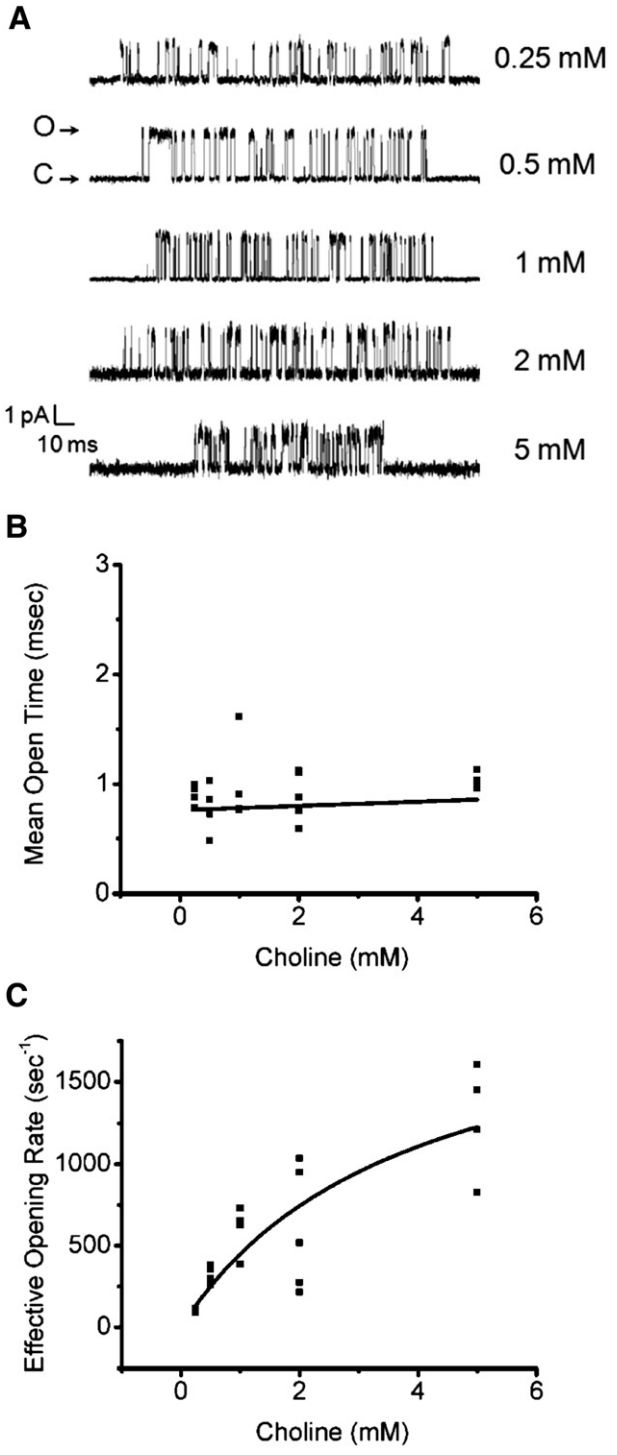

Fig. 4. Estimation of diliganded channel gating rate constants at high choline concentrations for the αG153S AChR. (A) Examples of single-channel clusters recorded at 0.25, 0.5, 1, 2, and 5 mM choline, shown at 10 kHz filtering with open events depicted as upward deflections. (B) A linear fit of the concentration dependence of intracluster mean open time yields $\alpha_2 = 1300 \pm 100\ s^{-1}$ and $K_{block} \sim 10^{-2}\ M^{-1}$. (C) Fitting the concentration dependence of the effective opening rate yields $\beta_2 = 2200 \pm 700\ s^{-1}$.

β_2', is the reciprocal of the major intracluster resting closed-time component that scales with agonist concentration. The dose response of β_2' was fitted to a Hill equation to estimate the true microscopic opening rate constant ($\beta_2 = 2200 \pm 700\ s^{-1}$) (Fig. 4B) [19,34,51]. The diliganded closing rate constant, α_2, was measured from the dose response of the mean open time τ_O. Choline is useful as a low-efficacy agonist that induces resolvable gating events, but fast open-

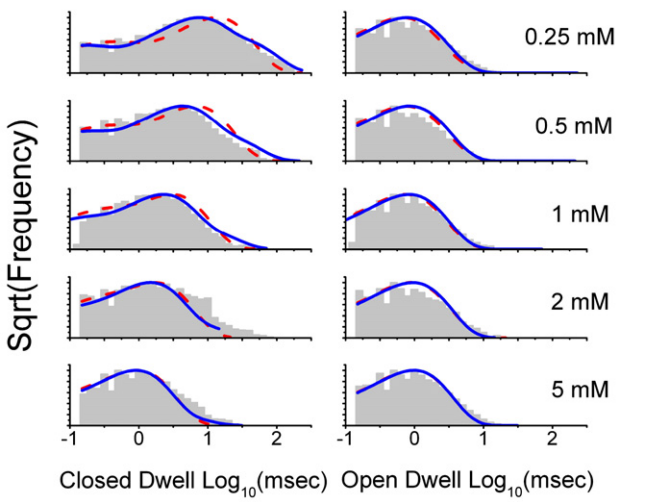

Fig. 5. Intracluster closed (left) and open (right) dwell-time distributions at 0.25, 0.5, 1, 2, and 5 mM choline. The maximum interval likelihood method was used to fit the data to Scheme 1 (red) or Scheme 2 (blue). Scheme 2 provides a statistically better fit.

channel blockade also occurs at high concentrations of this agonist. When fast blockade is present, the observed mean intracluster open time is $\tau_O = \alpha_2^{-1} + (\alpha_2 \cdot K_{Block})^{-1} \cdot [\text{choline}]$ (Fig. 4C) [34,52,53]. Using this relationship, the diliganded closing rate constant ($\alpha_2 = 1300 \pm 100\ s^{-1}$) and choline blocking equilibrium constant ($K_{Block} \sim 10^{-2}$ M) were determined. Fast choline block of the mutant is not different from the wild-type channel ($K_{Block} \sim$ 10–20 mM), as expected from the location of residue G153 in the binding site, far from the ion conduction pore. The concentration dependence of τ_o was observed to be shallow and linear, indicating that fast choline block is not severe up to 5 mM and is unlikely to skew rate constant estimation. Monoliganded openings still occur frequently at these concentrations, and they are included in the models for fitting. Only one monoliganded lifetime was observed above, and the monoliganded closing rate was therefore constrained to $\alpha_1 = 1900 \pm 100\ s^{-1}$ for both monoliganded open states in Scheme 2 during fitting. Unliganded openings are not

Table 2
Maximum interval likelihood rate estimation[a]

Scheme 1		Scheme 2	
k_+	1140000 ± 20000	k_+^L	2090000 ± 30000
k_-	1790 ± 20	k_-^L	5900 ± 100
		k_+^H	26000 ± 600
		k_-^H	9.3 ± 0.2
β_1	346 ± 4	β_1^L	524 ± 6
α_1	1900 ± 400[b]	α_1^L	1900 ± 400[b]
		β_1^H	50 ± 1
		α_1^H	1900 ± 400[b]
β_2	2200 ± 700[b]	β_2	2200 ± 700[b]
α_2	1300 ± 100[b]	α_2	1300 ± 100[b]
K_D	1560 ± 30	K_D^L	2820 ± 60
		K_D^H	360 ± 10
θ_1	0.18 ± 0.04	θ_1^L	0.28 ± 0.06
		θ_1^H	0.026 ± 0.006
θ_2	1.7 ± 0.6	θ_2	1.7 ± 0.6
LL	2543496	LL	2562125
Events	482898		
Clusters	9003		

[a] Association rate constants are in $M^{-1} \cdot s^{-1}$, and all other rate constants are s^{-1}. Dissociation constants are in μM, and equilibrium gating constants are unitless.
[b] Rate constants were fixed at measured values during fitting as explained in the text.

included in the models because they are extremely rare at the choline concentrations analyzed.

From maximum likelihood fitting of the constrained models, we determined that Scheme 2 was a statistically better descriptor than Scheme 1, and the fitted rate constants indicate closed-state choline affinities are distinct. The clusters of single-channel activity recorded at 0.25, 0.5, 1, 2, and 5 mM choline were simultaneously fitted to Scheme 1 or Scheme 2 using the maximum interval likelihood algorithm in the QuB software suite [19]. Both models were reasonably well fitted to the observed dwell time distributions (Fig. 5), consistent with the utility of Scheme 1 in scenarios where discrimination of the binding sites is not necessarily possible or important to the question at hand. However, the non-equivalent binding model is, for the results in the current study, a significantly better descriptor of the data statistically. Fitting Scheme 2 improved the log-likelihood score by 18936 compared to fitting Scheme 1 with only three additional free parameters. This difference is significant by the Schwartz criterion and likelihood-ratio tests ($\alpha = 0.001$) (Table 2) [3]. Therefore, the rate constant estimates from the fitted non-equivalent binding sites model (Scheme 2) were used for further analysis.

Rate estimates from fitting Scheme 2 show that the two TBSs have distinct resting closed-state binding and dissociation kinetics and differ in resting affinity by 10-fold (Table 2). For simplicity, the superscript labels "H" and "L" are used to indicate high and low affinity. The kinetics of choline association and dissociation differ substantially. The association rates differ by ~100-fold, with faster association to the low-affinity site ($k_+^H \sim 10^4\ M^{-1}\ s^{-1}$ versus $k_+^L \sim 10^6\ M^{-1}\ s^{-1}$). The dissociation rates differ by 1000-fold, with faster dissociation from the low-affinity site ($k_-^H \sim 10^1\ s^{-1}$ versus $k_-^L \sim 10^4\ s^{-1}$). The high-affinity binding site has a choline resting closed-state dissociation constant $K_D^H \sim 0.1$ mM, and the low-affinity site has a choline resting closed-state dissociation constant $K_D^L \sim 1$ mM.

In contrast, we estimate that the open-state choline dissociation constants are equivalent: $J_D^H \sim J_D^L \sim 50$ μM. Open-state association and dissociation rate constants are difficult to measure [54] and were not directly observed here. Instead, the open-state dissociation constants, J_D^L and J_D^H, can be determined by applying loop balance, a consequence of detailed balance, to the AChR conformational cycle (Scheme 3) [41]. Invoking loop balance, it follows that $K_D^L \cdot \Theta_1^H \cdot J_D^H = K_D^H \cdot \Theta_1^L \cdot J_D^L$. Using monoliganded gating equilibrium constants, $\Theta_1^L \sim 0.1$ and $\Theta_1^H \sim 0.01$, and resting closed-state affinities, we find that $J_D^L \sim J_D^H$. Loop balance allows us specifically to write expressions for J_D^L and J_D^H in terms of gating equilibrium constants and dissociation constants for the resting closed state: $J_D^L \cdot \Theta_2 = K_D^L \cdot \Theta_1^H$ and $J_D^H \cdot \Theta_2 = K_D^H \cdot \Theta_1^L$. Evaluating these expressions yields values of $J_D^L = 40 \pm 20$ μM and $J_D^H = 60 \pm 20$ μM. The TBSs are therefore functionally non-equivalent in the resting closed receptor ($K_D^H \sim 10 \cdot K_D^L$) and functionally equivalent in the open receptor ($J_D^H \sim J_D^L$).

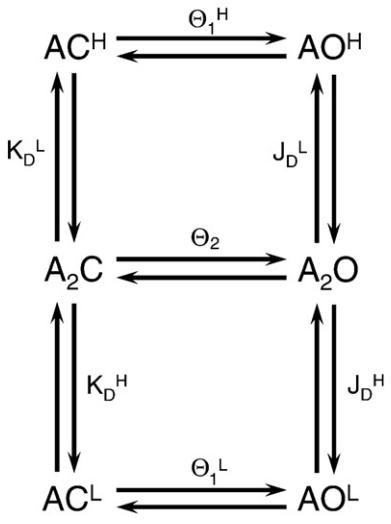

Scheme 3. AChR thermodynamic cycles. J_D^H and J_D^L are the open-state agonist dissociation constants. Because microscopic reversibility holds, loop balance can be applied. Thermodynamic loops that obey detailed balance: outer loop, $K_D^L \cdot \Theta_1^H \cdot J_D^H = K_D^H \cdot \Theta_1^L \cdot J_D^L$; top loop, $J_D^L \cdot \Theta_2 = K_D^L \cdot \Theta_1^H$; bottom loop, $J_D^H \cdot \Theta_2 = K_D^H \cdot \Theta_1^L$.

4. Discussion

4.1. State-dependent changes in binding site organization

Single-channel kinetic analysis of the αG153S AChR activated by choline has demonstrated that the two TBSs have non-equivalent resting-state affinities but equal open-state affinities. Structural data suggest that the channel subunits are non-uniformly oriented in the resting AChR: the two α subunits are rotated relative to the non-α subunits [7]. In contrast, all subunits have equivalent conformations in the open AChR, and the ligand-binding domains are equivalent with respect to the subunit orientation [14]. Our results suggest that there is a correlation between the subunit orientation, the structural organization of the two TBSs, and the function of the TBSs. Specifically, the binding sites have resting-state choline affinities which differ by 10-fold (~300 μM versus ~3000 μM) but have equivalent open-state choline affinities (~50 μM). While the functional results cannot provide independent confirmation of structural data, they are consistent with the predictions of structural studies in which the gating conformational change is associated with the α subunits making up a larger fraction of the TBSs compared to the δ and ε subunits.

Regardless of the state of the receptor, the differences in binding affinity and selectivity between the two TBSs may be attributed largely to residues on the complementary face in Loops D–G. Because the principal face is formed by α subunits at both binding sites, binding interactions between Loops A–C (which come from the α subunit) and the agonist are expected to be similar for the two sites. The complementary face is formed by the δ subunit at one TBS and the ε subunit at the other TBS. The non-equivalence of resting-state agonist affinities suggests that the complementary faces contribute appreciably to ligand–channel interactions. Several residues on the complementary face have been implicated in determining differential agonist and competitive antagonist affinities and specificities between the two sites in the closed AChR [21–23,25,26,55,56].

We observe that the TBSs have equal open-state affinities, suggesting that their principal faces increase their fractional contributions to agonist binding in the open state compared to the resting closed state (Fig. 1). In this explanation of the observed functional equivalence of binding sites, the fractional contributions of the complementary faces decrease in the open state so that the principal faces primarily determine open-state affinity. Currently, there are no models for the agonist-bound resting closed and open states of the intact receptor. The agonist-bound AChBP structures are thought to mimic the desensitized state of the intact receptor's TBSs, but it is not clear what differences exist between the open-state and desensitized state TBSs. However, our results are consistent with the hypothesis that structural models of the agonist-free resting closed state and the agonist-bound desensitized state are similar to the agonist-bound resting and open states, respectively. In X-ray crystal structures of carbamylcholine- or nicotine-bound AChBP, the agonist-buried surface area is approximately 2-fold greater for the principal face than the complementary face, suggesting that the agonist makes a larger number of contacts with the principal face [57]. The bound agonist may also be stabilized by closure of Loop C and compaction of the aromatic "cage", both α subunit components [7]. Our results are therefore also consistent with structural similarity between the open and desensitized states of the TBSs [58]. Both of these states are high affinity conformations with slow rates of agonist dissociation (0.1–10 s^{-1}) [25,26,54], and the binding affinities for the two TBSs in the

desensitized state are similar to each other [25,26]. While our functional studies suggest that the open-state and desensitized-state conformations of the transmitter binding sites are similar, a definitive answer to the question of open-state binding site conformation must await structural experiments that allow characterization of local residue environments in transient states. It may also be interesting to examine changes in binding site functional equivalence for binding of other agonists. Unlike acetylcholine, choline lacks a carbonyl moiety, which has been shown to be a pharmacophore. Thus, for quaternary ammonium containing cholinergic agonists, the charged moiety may be largely stabilized by the principal face, while the complementary face may have a larger fractional contribution to stabilization of the carbonyl and other uncharged moieties.

4.2. Conclusions and significance

The results of the kinetic experiments support the hypothesis that the αG153S AChR has unequal resting-state affinities and equal open-state affinities for choline. One explanation for the observed functional equivalence of TBSs in the open state is that open-state binding affinities are primarily determined by the α subunits and that the transmitter binding sites are structurally similar to one another in the open state. This explanation would further imply that the open- and desensitized-state TBS structures are not vastly different. The functional properties of the AChR therefore support the gating mechanism suggested by structural experiments, in which the transition to the open state is associated with an increase in orientational uniformity of the α subunits.

Appendix A. Supplementary data

Supplementary data associated with this article can be found, in the online version, at doi:10.1016/j.bbamem.2009.01.009.

References

[1] H.R. Arias, Localization of agonist and competitive antagonist binding sites on nicotinic acetylcholine receptors, Neurochem. Int. 36 (2000) 595–645.
[2] E.A. Gay, J.L. Yakel, Gating of nicotinic ACh receptors; new insights into structural transitions triggered by agonist binding that induce channel opening, J. Physiol. 584 (2007) 727–733.
[3] R.J. Prince, R.A. Pennington, S.M. Sine, Mechanism of tacrine block at adult human muscle nicotinic acetylcholine receptors, J. Gen. Physiol. 120 (2002) 369–393.
[4] S.M. Sine, A.G. Engel, Recent advances in Cys-loop receptor structure and function, Nature 440 (2006) 448–455.
[5] H.A. Lester, M.I. Dibas, D.S. Dahan, J.F. Leite, D.A. Dougherty, Cys-loop receptors: new twists and turns, Trends Neurosci. 27 (2004) 329–336.
[6] N. Zacharias, D.A. Dougherty, Cation–pi interactions in ligand recognition and catalysis, Trends Pharmacol. Sci. 23 (2002) 281–287.
[7] N. Unwin, Refined structure of the nicotinic acetylcholine receptor at 4Å resolution, J. Mol. Biol. 346 (2005) 967–989.
[8] K. Brejc, W.J. van Dijk, R.V. Klaassen, M. Schuurmans, J. van Der Oost, A.B. Smit, T.K. Sixma, Crystal structure of an ACh-binding protein reveals the ligand-binding domain of nicotinic receptors, Nature 411 (2001) 269–276.
[9] S.B. Hansen, G. Sulzenbacher, T. Huxford, P. Marchot, P. Taylor, Y. Bourne, Structures of *Aplysia* AChBP complexes with nicotinic agonists and antagonists reveal distinctive binding interfaces and conformations, EMBO J. 24 (2005) 3635–3646.
[10] C. Ulens, R.C. Hogg, P.H. Celie, D. Bertrand, V. Tsetlin, A.B. Smit, T.K. Sixma, Structural determinants of selective alpha-conotoxin binding to a nicotinic acetylcholine receptor homolog AChBP, Proc. Natl. Acad. Sci. U.S.A. 103 (2006) 3615–3620.
[11] C.D. Dellisanti, Y. Yao, J.C. Stroud, Z.Z. Wang, L. Chen, Crystal structure of the extracellular domain of nAChR alpha1 bound to alpha-bungarotoxin at 1.94 Å resolution, Nat. Neurosci. 10 (2007) 953–962.
[12] R.J. Hilf, R. Dutzler, X-ray structure of a prokaryotic pentameric ligand-gated ion channel, Nature 452 (2008) 375–379.
[13] G. Wilson, A. Karlin, Acetylcholine receptor channel structure in the resting, open, and desensitized states probed with the substituted-cysteine-accessibility method, Proc. Natl. Acad. Sci. U.S.A. 98 (2001) 1241–1248.
[14] N. Unwin, Acetylcholine receptor channel imaged in the open state, Nature 373 (1995) 37–43.
[15] D.P. Tieleman, P.C. Biggin, G.R. Smith, M.S. Sansom, Simulation approaches to ion channel structure-function relationships, Q. Rev. Biophys. 34 (2001) 473–561.
[16] X. Liu, Y. Xu, H. Li, X. Wang, H. Jiang, F.J. Barrantes, Mechanics of channel gating of the nicotinic acetylcholine receptor, PLoS Comp. Biol. 4 (2008) e19.
[17] X. Cheng, I. Ivanov, H. Wang, S.M. Sine, J.A. McCammon, Nanosecond-timescale conformational dynamics of the human alpha7 nicotinic acetylcholine receptor, Biophys. J. 93 (2007) 2622–2634.
[18] S.M. Sine, T. Claudio, F.J. Sigworth, Activation of *Torpedo* acetylcholine receptors expressed in mouse fibroblasts. Single channel current kinetics reveal distinct agonist binding affinities, J. Gen. Physiol. 96 (1990) 395–437.
[19] F.N. Salamone, M. Zhou, A. Auerbach, A re-examination of adult mouse nicotinic acetylcholine receptor channel activation kinetics, J. Physiol. 516 (1999) 315–330.
[20] S.M. Sine, K. Ohno, C. Bouzat, A. Auerbach, M. Milone, J.N. Pruitt, A.G. Engel, Mutation of the acetylcholine receptor alpha subunit causes a slow-channel myasthenic syndrome by enhancing agonist binding affinity, Neuron 15 (1995) 229–239.
[21] P. Blount, J.P. Merlie, Molecular basis of the two nonequivalent ligand binding sites of the muscle nicotinic acetylcholine receptor, Neuron 3 (1989) 349–357.
[22] P. Blount, J.P. Merlie, Characterization of an adult muscle acetylcholine receptor subunit by expression in fibroblasts, J. Biol. Chem. 266 (1991) 14692–14696.
[23] B.E. Molles, I. Tsigelny, P.D. Nguyen, S.X. Gao, S.M. Sine, P. Taylor, Residues in the epsilon subunit of the nicotinic acetylcholine receptor interact to confer selectivity of waglerin-1 for the alpha-epsilon subunit interface site, Biochemistry 41 (2002) 7895–7906.
[24] R.J. Prince, S.M. Sine, Epibatidine activates muscle acetylcholine receptors with unique site selectivity, Biophys. J. 75 (1998) 1817–1827.
[25] K.L. Martinez, P.J. Corringer, S.J. Edelstein, J.P. Changeux, F. Merola, Structural differences in the two agonist binding sites of the *Torpedo* nicotinic acetylcholine receptor revealed by time-resolved fluorescence spectroscopy, Biochemistry 39 (2000) 6979–6990.
[26] I.E. Andreeva, S. Nirthanan, J.B. Cohen, S.E. Pedersen, Site specificity of agonist-induced opening and desensitization of the *Torpedo californica* nicotinic acetylcholine receptor, Biochemistry 45 (2006) 195–204.
[27] M. Zhou, A.G. Engel, A. Auerbach, Serum choline activates mutant acetylcholine receptors that cause slow channel congenital myasthenic syndromes, Proc. Natl. Acad. Sci. U.S.A. 96 (1999) 10466–10471.
[28] C. Grosman, A. Auerbach, Asymmetric and independent contribution of the second transmembrane segment 12' residues to diliganded gating of acetylcholine receptor channels: a single-channel study with choline as the agonist, J. Gen. Physiol. 115 (2000) 637–651.
[29] Y. Purohit, C. Grosman, Block of muscle nicotinic receptors by choline suggests that the activation and desensitization gates act as distinct molecular entities, J. Gen. Physiol. 127 (2006) 703–717.
[30] P. Purohit, A. Mitra, A. Auerbach, A stepwise mechanism for acetylcholine receptor channel gating, Nature 446 (2007) 930–933.
[31] C. Grosman, M. Zhou, A. Auerbach, Mapping the conformational wave of acetylcholine receptor channel gating, Nature 403 (2000) 773–776.
[32] S.M. Sine, Molecular dissection of subunit interfaces in the acetylcholine receptor: identification of residues that determine curare selectivity, Proc. Natl. Acad. Sci. U.S.A. 90 (1993) 9436–9440.
[33] O.P. Hamill, A. Marty, E. Neher, B. Sakmann, F.J. Sigworth, Improved patch-clamp techniques for high-resolution current recording from cells and cell-free membrane patches, Pflugers Arch. 391 (1981) 85–100.
[34] B. Sakmann, E. Neher, Single-Channel Recording, 2nd ed. Plenum Press, New York, 1995.
[35] F. Qin, Restoration of single-channel currents using the segmental k-means method based on hidden Markov modeling, Biophys. J. 86 (2004) 1488–1501.
[36] F. Qin, A. Auerbach, F. Sachs, Estimating single-channel kinetic parameters from idealized patch-clamp data containing missed events, Biophys. J. 70 (1996) 264–280.
[37] F. Qin, Restoration of single-channel currents using the segmental k-means method based on hidden Markov modeling, Biophys. J. 86 (2004) 1488–1501.
[38] F. Qin, A. Auerbach, F. Sachs, Maximum likelihood estimation of aggregated Markov processes, Proc. R. Soc. B. 264 (1997) 375–383.
[39] F. Qin, L. Li, Model-based fitting of single-channel dwell-time distributions, Biophys. J. 87 (2004) 1657–1671.
[40] A. Auerbach, C.J. Lingle, Heterogeneous kinetic properties of acetylcholine receptor channels in *Xenopus* myocytes, J. Physiol. 378 (1986) 119–140.
[41] D. Colquhoun, B. Sakmann, Fast events in single-channel currents activated by acetylcholine and its analogues at the frog muscle end-plate, J. Physiol. 369 (1985) 501–557.
[42] G. Akk, S. Sine, A. Auerbach, Binding sites contribute unequally to the gating of mouse nicotinic alpha D200N acetylcholine receptors, J. Physiol. 496 (1996) 185–196.
[43] D.J. Cadugan, A. Auerbach, Conformational dynamics of the alphaM3 transmembrane helix during acetylcholine receptor channel gating, Biophys. J. 93 (2007) 859–865.
[44] A. Mitra, T.D. Bailey, A.L. Auerbach, Structural dynamics of the M4 transmembrane segment during acetylcholine receptor gating, Structure 12 (2004) 1909–1918.
[45] A. Mitra, G.D. Cymes, A. Auerbach, Dynamics of the acetylcholine receptor pore at the gating transition state, Proc. Natl. Acad. Sci. U.S.A. 102 (2005) 15069–15074.
[46] M. Milone, H.L. Wang, K. Ohno, T. Fukudome, J.N. Pruitt, N. Bren, S.M. Sine, A.G. Engel, Slow-channel myasthenic syndrome caused by enhanced activation, desensitization, and agonist binding affinity attributable to mutation in the M2 domain of the acetylcholine receptor alpha subunit, J. Neurosci. 17 (1997) 5651–5665.

[47] G. Akk, A. Auerbach, Activation of muscle nicotinic acetylcholine receptor channels by nicotinic and muscarinic agonists, Br. J. Pharmacol. 128 (1999) 1467–1476.
[48] C.J. Hatton, C. Shelley, M. Brydson, D. Beeson, D. Colquhoun, Properties of the human muscle nicotinic receptor, and of the slow-channel myasthenic syndrome mutant epsilonL221F, inferred from maximum likelihood fits, J. Physiol. 547 (2003) 729–760.
[49] G. Akk, M. Zhou, A. Auerbach, A mutational analysis of the acetylcholine receptor channel transmitter binding site, Biophys. J. 76 (1999) 207–218.
[50] R. Lape, D. Colquhoun, L.G. Sivilotti, On the nature of partial agonism in the nicotinic receptor superfamily, Nature 454 (2008) 722–727.
[51] A. Auerbach, A statistical analysis of acetylcholine receptor activation in *Xenopus* myocytes: stepwise versus concerted models of gating, J. Physiol. 461 (1993) 339–378.
[52] A. Auerbach, G. Akk, Desensitization of mouse nicotinic acetylcholine receptor channels. A two-gate mechanism, J. Gen. Physiol. 112 (1998) 181–197.
[53] S. Elenes, A. Auerbach, Desensitization of diliganded mouse muscle nicotinic acetylcholine receptor channels, J. Physiol. 541 (2002) 367–383.
[54] C. Grosman, A. Auerbach, The dissociation of acetylcholine from open nicotinic receptor channels, Proc. Natl. Acad. Sci. U.S.A. 98 (2001) 14102–14107.
[55] A. Karlin, Emerging structure of the nicotinic acetylcholine receptors, Nat. Rev. Neurosci. 3 (2002) 102–114.
[56] R.J. Prince, S.M. Sine, Molecular dissection of subunit interfaces in the acetylcholine receptor. Identification of residues that determine agonist selectivity, J. Biol. Chem. 271 (1996) 25770–25777.
[57] P.H. Celie, S.E. van Rossum-Fikkert, W.J. van Dijk, K. Brejc, A.B. Smit, T.K. Sixma, Nicotine and carbamylcholine binding to nicotinic acetylcholine receptors as studied in AChBP crystal structures, Neuron 41 (2004) 907–914.
[58] D.S. Stewart, D.C. Chiara, J.B. Cohen, Mapping the structural requirements for nicotinic acetylcholine receptor activation by using tethered alkyltrimethylammonium agonists and antagonists, Biochemistry 45 (2006) 10641–10653.